Parametric correlations of local density-of-states fluctuations in disordered pillars, wires and films

2001 J. Phys.: Condens. Matter 13 6633

(http://iopscience.iop.org/0953-8984/13/31/305)

INSTITUTE OF PHYSICS PUBLISHING JOURNAL OF PHYSICS: CONDENSED MATTER

J. Phys.: Condens. Matter **13** (2001) 6633–6648 PII: S0953-8984(01)23977-0

Parametric correlations of local density-of-states fluctuations in disordered pillars, wires and films

Edward McCann and Vladimir I Fal'ko

Department of Physics, Lancaster University, Lancaster LA1 4YB, UK

Received 18 April 2001, in final form 19 June 2001
Published 19 July 2001
Online at stacks.iop.org/JPhysCM/13/6633

Abstract

We present a theoretical analysis of correlation properties of the local density of states in a disordered emitter probed by resonant tunnelling through a localized impurity state. The emitter is considered to be a cylinder of length L and radius R with elastic mean free path $l \ll \{L, R\}$ and the effective dimensionality $d \leqslant 3$ of the emitter is determined by the relation between the typical scale over which diffusion occurs, namely the quasi-particle relaxation length L_c, and the dimensions L and R. The differential conductance measured in asymmetric double-barrier structures has been used (see, e.g., Schmidt T, Haug R J, Fal'ko V I, von Klitzing K, Förster A and Lüth H 1996 *Europhys. Lett.* **36** 61) to image local density-of-states fluctuations. We give analytic expressions for the variance and for correlations of the differential conductance with respect to voltage and applied magnetic field for the limits of a bulk three-dimensional emitter, a film, a wire and a pillar, and we determine the effect of magnetic anisotropy in lower dimensions. A numerical calculation, valid for arbitrary L_c, is performed in order to describe the crossovers between these limits where the correlation functions are sensitive to the shape of the emitter and the position of the resonant impurity.

1. Introduction

A number of vertical transport experiments on double-barrier semiconductor heterostructures [1–5] have observed impurity-assisted tunnelling, providing the possibility of using the resonant impurity level as a local probe of electronic states of the electrodes. In particular, the current $I(V)$ and differential conductance $G = \mathrm{d}I/\mathrm{d}V$ measured in strongly asymmetric double-barrier structures have been used to image fluctuations of the local density of states (LDOS) of an electrode as a function of excitation energy E from the Fermi level [5–11]. Measurements taken for a series of applied magnetic field values produce a large statistical ensemble of fluctuation data, $\delta G(V, B) = G(V, B) - \langle G \rangle$, allowing a comparison of experimentally determined correlation functions [5, 11] with theoretical predictions [12].

0953-8984/01/316633+16$30.00

Mesoscopic fluctuations of the local density of states (LDOS) in disordered systems are believed to exhibit a broad distribution even in the metallic regime [13–15]. The fluctuations arise from the quantum interference of electrons that are multiply scattered off an impurity potential, characterized by an elastic mean free path l, resulting in coherent diffusion within a volume limited by a quasi-particle relaxation length L_c. When the diffusion of the electron density is damped before it is able to cover the whole length L of the sample, $L_c \ll L$, the exact geometry of the sample is irrelevant and it is possible to integrate over all harmonics of diffusive modes, neglecting discreteness caused by particular boundary conditions. On the other hand, when the electron density diffuses throughout the entire system, $L \ll L_c$, the lowest harmonic of the diffusive mode is divergent and it is possible to neglect the contribution of higher harmonics [16–18], a procedure known as the zero-mode approximation. Therefore the effective dimensionality of a sample, as far as mesoscopic fluctuations are concerned, is determined by the relation between L_c and L, and, when L_c is comparable with L, the magnitude of fluctuations and the form of correlation functions depend on the sample geometry.

In this paper we present a detailed quantitative analysis of correlation properties of the differential conductance of an asymmetric double-barrier structure for various effective dimensionalities in order to provide a theoretical basis for a quantitative comparison with fluctuation data obtained experimentally. To model a typical experimental geometry [5,6,9–11] we consider a nominally three-dimensional electrode which is a cylinder of length L and radius R as sketched in figure 1 (cross sectional area $S = \pi R^2$). Tunnelling via an impurity state of energetic width Γ gives $L_c = \sqrt{\hbar D/(\Gamma + \hbar\gamma)}$ where $D = v_F l/3$ is the diffusion coefficient of the electrode and γ is a quasi-particle relaxation rate due to processes within it. Thus the effective dimensionality of observed fluctuations is determined by the geometry of the emitter, the resonant impurity width and the strength of quasi-particle relaxation. The large amount of data obtained in recent experiments enables one to make a statistically sound analysis of correlation functions of fluctuations and to extract information about the emitter including the efficiency of electron–electron interaction-induced relaxation of a hole below the Fermi level created after the tunnelling event [10, 11].

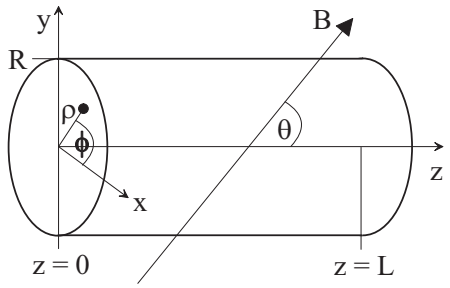

Figure 1. A sketch of the geometry of the emitter which is a cylinder of length L and radius R. The resonant impurity is situated at one end $z = 0$ at a finite radius ρ away from the cylinder axis and the applied magnetic field B may generally be directed at a tilt angle θ with respect to the cylinder axis.

In principle, it is possible to imagine four different limiting relationships between the lengths L, R and L_c which correspond to different effective dimensionalities $d \leqslant 3$. The limits include bulk three-dimensional (3D) and quasi-d-dimensional (QdD) ones for $d = \{0, 1, 2\}$ as summarized in table 1. In the geometry we consider the current flow is along the cylinder (the z-axis) which is perpendicular to the plane of a film for Q2D and along a wire for Q1D. One way to distinguish between the limiting cases is by means of magnetic field anisotropy.

Table 1. Definitions of the limits of effective dimensionality in terms of the relation between the relaxation length L_c and the emitter dimensions L and R.

Effective dimensionality	Relation of lengths	Description
3D	$L_c \ll \{R, L\}$	Bulk three dimensional
Q2D	$L \ll L_c \ll R$	Thin film
Q1D	$R \ll L_c \ll L$	Wire
Q0D	$\{R, L\} \ll L_c$	Pillar

As stated above, in the 3D limit the exact geometry of the electrode is irrelevant because diffusion is damped before the boundaries are reached and in this case there is no dependence on the orientation of an applied magnetic field. In other limiting cases, however, when many harmonics contribute in some directions and the zero mode dominates in other directions, there is anisotropy with respect to an applied magnetic field.

A particular experimental realization is likely to correspond to a value of L_c somewhere between the idealized limiting cases. In this situation the diffusive modes are composed of many harmonics that are sensitive to the exact geometry of the emitter and the position of the resonant impurity (spectrometer) with respect to it. We take this into account by numerically solving the diffusion equation in the presence of the boundary conditions for a cylinder for various values of L, R and L_c, and different positions of the spectrometer.

The paper is organized as follows. In section 2 we show how to relate the fluctuations of the differential conductance to diffusive modes and we present analytic results for the variance in the limiting cases defined in table 1. Section 3 describes the calculation of the voltage-dependent correlations, giving both analytic results in the limiting cases and numerical results for the crossovers between them. Finally, in section 4 we present analytic results for magnetic field-dependent correlations, taking into account magnetic field anisotropy.

2. Differential conductance fluctuations

In the experiments on asymmetric double-barrier structures [5–11] electrons tunnel from a heavily doped disordered emitter through the energetically lowest level E_S in the quantum well sandwiched between the barriers, the level serving as a spectrometer of the emitter. At zero bias, the energy of the discrete impurity level E_S does not coincide with the bulk chemical potential μ_l and it comes to resonance only after the bias voltage reaches a threshold value $V_S(E_S)$. The current–voltage $I(V)$ characteristics of such a device can be divided into three typical intervals [2–5, 19]: below the threshold, where $I \approx 0$; the threshold regime $V \approx V_S(E_S)$, where $I(V)$ undergoes a jump when the resonant level crosses the Fermi level μ_l in the emitter; and the interval of a plateau, $V_S(E_S) < V < V_1(E_1)$, where the current remains nearly constant until the next impurity level E_1 is lowered enough to contribute to the transport. Observed variations of the $I(V)$ characteristics on the plateau can only be due to the energy dependence of an electron below the Fermi level in the emitter which makes the plateau regime ideal for studying the image of LDOS fluctuations in the current.

The aim of the theory is to calculate the correlation function of two differential conductances taken at different voltages and magnetic fields and to separate it into the product of the variance and a normalized correlation function $K(\Delta V, \Delta B)$,

$$\langle \delta G(V, B)\, \delta G(V', B') \rangle = \langle (\delta G)^2 \rangle K(\Delta V, \Delta B) \tag{1}$$

where $\Delta V = V' - V$, $\Delta B = B' - B$ and $K(0,0) = 1$. We begin by briefly showing how to write the correlation function in terms of Green's functions and for further details we refer the reader to reference [12] which considered the limits of 3D and Q2D emitters. The current is expressed in terms of the rates of tunnelling through the thick barrier on the emitter side, denoted Γ_l, and the thin barrier on the collector side, Γ_r, using the single-particle Breit–Wigner resonance conductance formula [20–23]:

$$I(V) \approx \frac{e}{h}\int_{-\infty}^{\infty} \frac{\Gamma_l(\epsilon)\Gamma_r(\epsilon)\,[f_l(\epsilon) - f_r(\epsilon)]\ \mathrm{d}\epsilon}{[\epsilon - \epsilon_0(V)]^2 + \Gamma^2(\epsilon)/4} \tag{2}$$

where

$$f_{l(r)}(\epsilon) = \{1 + \exp[(\epsilon - \mu_{l(r)})/T]\}^{-1}$$

and we have neglected electron spin, although the final answers will be normalized so that this is taken into account. The total width is $\Gamma = \Gamma_l + \Gamma_r$ and in the case that we study here $\Gamma_r \gg \Gamma_l$, so $\Gamma \approx \Gamma_r$. Experimentally, such asymmetry arises from the structure of the sample studied. In references [9–11], for example, the structure consists of a 10 nm wide GaAs quantum well sandwiched between two $Al_{0.3}Ga_{0.7}As$ barriers of 5 and 8 nm width, making the transparency of the thick emitter barrier orders of magnitude lower than that of the collector barrier.

The height of the resonance conductance peak, G_Γ, may be obtained from equation (2) by setting $\mu_l \approx \epsilon_0(V)$:

$$G_\Gamma = \left\langle \frac{\mathrm{d}I}{\mathrm{d}V} \right\rangle_{\max} \approx \frac{4\alpha e^2}{h}\frac{\Gamma_l}{\Gamma_r} \tag{3}$$

and the width at half-maximum is $V_\Gamma \approx \Gamma/(e\alpha)$. The voltage-to-energy conversion factor $\alpha < 1$ takes into account the actual distribution of the potential drop across the sample. The average current in the plateau regime may be found from equation (2) by taking the limit $(\mu_l - \epsilon_0) \gg \{\Gamma, T\}$:

$$\langle I \rangle \approx 2e\pi\Gamma_l/h \tag{4}$$

so the ensemble average $\langle \mathrm{d}I/\mathrm{d}V \rangle$ tends to zero on the plateau.

The sample-specific fine structure of the current on the plateau is characterized by the disorder-averaged correlation function of currents measured at different voltages $\langle \delta I(V)\, \delta I(V') \rangle$. It is dominated by fluctuations of the rate of tunnelling Γ_l between the impurity and the continuum of states below the Fermi level μ_l of the disordered emitter, whereas fluctuations of the rate of tunnelling between the impurity and collector $\Gamma_r \approx \Gamma$ are neglected for quantitative reasons resulting from the asymmetry of the device $\Gamma_r \gg \Gamma_l$ and because, at high voltages, quantum interference effects in the collector are washed out by electron–electron collisions and the emission of plasmons and optical phonons. One considers a product of tunnelling rates at energies ϵ and ϵ', with resonant energies ϵ_0 and ϵ_0' respectively, and, after changing variables as follows:

$$\omega = (\epsilon' - \epsilon) \qquad E = (\epsilon' + \epsilon)/2$$
$$\Omega = (\epsilon_0' - \epsilon_0) \approx \alpha e(V' - V) \qquad E_0 = (\epsilon_0' + \epsilon_0)/2$$

the current correlator may be written, using equation (2), as

$$\langle \delta I(V,B)\, \delta I(V',B') \rangle \approx \left(\frac{e\Gamma}{h}\right)^2 \int_{-\infty}^{\infty}\int_{-\infty}^{\infty} \mathrm{d}\omega\, \mathrm{d}E \prod_{\pm} \frac{1}{(E \pm \omega/2 - E_0 \mp \Omega/2)^2 + \Gamma^2/4}$$
$$\times \left\langle \delta\Gamma_l\left(E - \frac{\omega}{2}, B\right) \delta\Gamma_l\left(E + \frac{\omega}{2}, B'\right) \right\rangle. \tag{5}$$

The variation of the current at high energy (voltage) scales is sensitive to electron dynamics at short distances near the resonant impurity. That creates an uncertainty in the estimation of the r.m.s. value of the current fluctuations and impedes quantitative description of the observed features of the $I(V)$ characteristics since a rigorous calculation of the current–current correlator becomes model dependent. On the other hand, such a deficiency does not affect the correlation functions of two differential conductances, where the contribution of faster energy dependences (longer length scales) is enhanced by the differentiation procedure. Such a correlation function can be obtained from the disordered averaged current–current correlation function [13] by taking the second derivative with respect to $\Omega = \alpha e(V - V')$:

$$\langle \delta G(V, B)\, \delta G(V', B') \rangle = -(\alpha e)^2 \frac{\partial^2}{\partial \Omega^2} \langle \delta I(V, B)\, \delta I(V', B') \rangle.$$

Integrating equation (5) with respect to E one may write

$$\langle \delta G(V, B)\, \delta G(V', B') \rangle \approx -4\pi\Gamma \left(\frac{\alpha e^2}{h}\right)^2 \frac{\partial^2}{\partial \Omega^2} \int_{-\infty}^{\infty} \frac{\langle \delta\Gamma_l(-\omega/2, B)\, \delta\Gamma_l(\omega/2, B') \rangle \, \mathrm{d}\omega}{\left[(\omega - \Omega)^2 + \Gamma^2\right]}. \quad (6)$$

The disorder-averaged product of tunnelling rates $\langle \delta\Gamma_l(E - \omega/2, B)\, \delta\Gamma_l(E + \omega/2, B') \rangle$ is independent of E and dominated by contributions from diffusive modes that are singular as $\omega \to 0$. To demonstrate this, the tunnelling rate is written in terms of the exact retarded (advanced) Green's functions of the electrode $\mathcal{G}^{R\,(A)}$ [12, 23]:

$$\Gamma_l(\epsilon) \approx 2\,|t|^2 \int \frac{\mathrm{d}\boldsymbol{p}}{(2\pi)^d}\, \mathrm{Im}[\mathcal{G}^A_\epsilon(\boldsymbol{p})] \quad (7)$$

where $\mathrm{Im}[\mathcal{G}^A] = [\mathcal{G}^A - \mathcal{G}^R]/2$ and t is the tunnelling matrix element connecting the impurity and the bulk electrode; its exact form plays no part in the following analysis. Equations (6) and (7) show that correlations of the differential conductance are determined by correlations of the local density of states in the emitter. After using the standard diagrammatic perturbation theory techniques, which are eligible when applied to metallic systems with $k_F l \gg 1$ and a continuous energy spectrum [18], $\langle \delta\Gamma_l(-\omega/2, B)\, \delta\Gamma_l(+\omega/2, B') \rangle$ can be represented in terms of diffusion modes $P_\omega(\boldsymbol{r}, \boldsymbol{r})$:

$$\left\langle \delta\Gamma_l\left(-\frac{\omega}{2}, B\right) \delta\Gamma_l\left(+\frac{\omega}{2}, B'\right) \right\rangle \approx \frac{1}{2\pi\nu\tau^2} \left(\frac{2}{\beta}\right) \int \frac{\mathrm{d}\boldsymbol{q}}{(2\pi)^d} \left[P_\omega(\boldsymbol{q}) + P_{-\omega}(\boldsymbol{q})\right] \times \left[|t|^2 \int \frac{\mathrm{d}\boldsymbol{p}}{(2\pi)^d} \left\langle \mathcal{G}^A_E\left(\boldsymbol{p} + \frac{\boldsymbol{q}}{2}\right)\right\rangle \left\langle \mathcal{G}^R_E\left(\boldsymbol{p} - \frac{\boldsymbol{q}}{2}\right)\right\rangle\right]^2 \quad (8)$$

where τ is the mean elastic scattering time in the emitter and

$$\langle \mathcal{G}^{R\,(A)}_E(\boldsymbol{p}) \rangle = [E - \epsilon(p) \pm \mathrm{i}\hbar/(2\tau)]^{-1}$$

is the ensemble-averaged single-particle Green's function. In the absence of time-reversal symmetry, $\langle (\delta\Gamma_l)^2 \rangle$ is reduced by the standard Dyson's factor of $1/\beta$, where $\beta = 1$ for the orthogonal ensemble (in the presence of impurity scattering only) and $\beta = 2$ for the unitary ensemble (in the presence of a finite magnetic field or weak scattering by magnetic impurities that breaks time-reversal invariance). In the language of diagrammatics, diffusion and Cooperon propagators give the same contribution at zero magnetic field, but Cooperon propagators are excluded when time-reversal symmetry is broken. Thus, in terms of diffusion propagators, the correlation function takes the form [12]

$$\langle \delta G(V)\, \delta G(V') \rangle = -\frac{1}{\beta} \left(\frac{\alpha e^2 \Gamma_l}{\pi\hbar}\right)^2 \left(\frac{\partial^2}{\partial \Omega^2}\right) \frac{\Gamma}{\nu} \int \frac{\mathrm{d}\omega \left[P_\omega(\boldsymbol{r}, \boldsymbol{r}) + P_{-\omega}(\boldsymbol{r}, \boldsymbol{r})\right]}{(\hbar\omega - \Omega)^2 + \Gamma^2} \quad (9)$$

where $\boldsymbol{r}$ is the coordinate of the resonant impurity and P satisfies the diffusion equation [24]

$$\left[-D\left(\boldsymbol{\nabla}-\frac{\mathrm{i}e}{\hbar c}\boldsymbol{A}\right)^2+\gamma-\mathrm{i}\omega\right]P_\omega(\boldsymbol{r},\boldsymbol{r}')=\delta(\boldsymbol{r}-\boldsymbol{r}') \tag{10}$$

where rot $\boldsymbol{A}=\Delta\boldsymbol{B}$. The propagator $P_\omega(\boldsymbol{r},\boldsymbol{r}')$ describes diffusion in a half-space restricted by the tunnelling barrier at $z=0$ and an insulating boundary at the cylinder surface $\rho=R$. We consider there to be a tunnelling barrier at the emitter–substrate interface $z=L$, although this allows us to model a good emitter–substrate interface by taking $L\to\infty$. In the presence of a vector potential the boundary condition at a tunnelling barrier is [17]

$$\boldsymbol{n}\cdot(\boldsymbol{\nabla}-\boldsymbol{A})\psi=0 \tag{11}$$

where $\boldsymbol{n}$ is the normal to the surface.

The variance may be found by setting $\Delta V=0$ and $\Delta B=0$, and, in the limits of the effective dimensionalities defined in table 1, the diffusion propagator may be calculated analytically. In this case the exact shape of the cross section of the emitter is not important, so we consider a case that is easy to model, namely a 'cylinder' of length L in the z-direction with a square cross section of area $S=L_\perp^2$ in the (x,y) directions. For the impurity positioned on the axis of the emitter, $\rho=0$, we find

$$P_\omega(\boldsymbol{r},\boldsymbol{r})=\frac{1}{LS}\sum_{\boldsymbol{q}_\perp}\sum_{q_z}\frac{2\cos^2(q_z z)}{(Dq^2+\gamma-\mathrm{i}\omega)} \tag{12}$$

where the momentum $\boldsymbol{q}$ is expressed in terms of components along the cylinder axis q_z and perpendicular to the axis $\boldsymbol{q}_\perp$ giving $q^2=q_z^2+q_\perp^2$. The boundary condition (11) gives $q_z=n_z\pi/L$ where $n_z=0,1,2,\ldots$ and $\boldsymbol{q}_\perp=\{2n_x\pi/L_\perp,2n_y\pi/L_\perp\}$ where $n_{x(y)}=0,\pm1,\pm2,\ldots$. When the relaxation length L_c is much shorter than a particular dimension of the emitter, L_i for $i=\{x,y,z\}$, then electrons typically cannot diffuse across the sample within the relaxation time. It is possible to assume that the emitter is very long in that direction so that the discreteness of momenta is irrelevant, allowing one to approximate the summation in equation (12) by an integration over all corresponding components of momenta q_i. On the other hand, when $L_c\gg L_i$ then a typical electron can diffuse across the sample within the relaxation time. In this case the lowest mode $q_i=0$ gives the dominant contribution to the propagator (12). For example, for a 3D emitter, $\{L,R\}\gg L_c$, one integrates with respect to momenta perpendicular to the axis of the cylinder and along the axis [12]:

$$P_\omega(\boldsymbol{r},\boldsymbol{r})=\int\frac{\mathrm{d}\boldsymbol{q}_\perp}{(2\pi)^2}\int_0^\infty\frac{\mathrm{d}q_z}{\pi}\,\frac{2\cos^2(q_z z)}{(Dq^2+\gamma-\mathrm{i}\omega)}. \tag{13}$$

Other effective dimensionalities d correspond to cases where $3-d$ of the sample dimensions are smaller than L_c, in which case the summation in equation (12) is performed by making integrations in d directions and retaining the lowest mode in $3-d$ directions. For Q2D geometry, $R\gg L_c\gg L$, one integrates with respect to $q_\perp$ but keeps only $q_z=0$, whereas for Q1D, $L\gg L_c\gg R$, one integrates with respect to q_z and keeps only $q_\perp=0$. Finally for Q0D, $L_c\gg\{L,R\}$, one keeps $q_z=0$ and $q_\perp=0$ only. Expressions for the variance of the differential conductance fluctuations for quasi-dimensionality $d=\{3,2,1,0\}$ are obtained by setting $\Delta V=0$:

$$\langle(\delta G_3)^2\rangle=\frac{\sqrt{\Gamma}}{16\beta\nu(\hbar D)^{3/2}}\frac{G_\Gamma^2}{[1+\hbar\gamma/\Gamma]^{3/2}} \tag{14}$$

$$\langle(\delta G_2)^2\rangle=\frac{1}{8\beta\nu\hbar DL}\frac{G_\Gamma^2}{[1+\hbar\gamma/\Gamma]^2} \tag{15}$$

$$\langle(\delta G_1)^2\rangle = \frac{3\pi}{8\beta\nu S\sqrt{\hbar D\Gamma}}\frac{G_\Gamma^2}{[1+\hbar\gamma/\Gamma]^{5/2}} \tag{16}$$

$$\langle(\delta G_0)^2\rangle = \frac{\pi}{\beta\nu\Gamma LS}\frac{G_\Gamma^2}{[1+\hbar\gamma/\Gamma]^3}. \tag{17}$$

The variance is normalized by G_Γ^2 in order to show that it is parametrically suppressed as compared to the square of the height of the main peak. Since we consider d quasi-dimensions embedded in a three-dimensional space, the suppression factor is $1/(g(L_\Gamma)L^{3-d})$ where $g(L_\Gamma)$ is the conductance (measured in units of e^2/h) of a d-dimensional piece of electrode with length equal to L_Γ [12], $g(L_\Gamma) \sim \nu\Gamma L_\Gamma^d$.

3. Voltage-dependent correlation functions

Limiting expressions for voltage correlations are obtained in the same way as those for the variance, keeping $\Delta B = 0$ but with ΔV non-zero:

$$K_3(\Delta V, 0) = \frac{(2-Y)\sqrt{1+Y)}}{\sqrt{2}Y^3} \qquad Y = \sqrt{1+\left(\frac{\Delta V}{V_c}\right)^2} \tag{18}$$

$$K_2(\Delta V, 0) = \frac{1-(\Delta V/V_c)^2}{\left[1+(\Delta V/V_c)^2\right]^2} \tag{19}$$

$$K_1(\Delta V, 0) = \frac{(4-2Y-Y^2)\sqrt{1+Y}}{\sqrt{2}Y^5} \tag{20}$$

$$K_0(\Delta V, 0) = \frac{1-3(\Delta V/V_c)^2}{\left[1+(\Delta V/V_c)^2\right]^3}. \tag{21}$$

Typical correlation voltages which can be observed in the experiment may differ from the width of the main conductance resonance only by the relaxation rate γ of a floating-up 'hole' below the Fermi level created in the emitter after the tunnelling event, $V_c = V_\Gamma + \hbar\gamma/(\alpha e)$. The form of the correlation function $K_d(\Delta V, 0)$ in the four different effective dimensionalities considered above is plotted in figure 2. Parameters which give a quantitative measure of the shape of the correlation function, the half-width V_K, the voltage at the first minimum $V_{\min}$ and the value of the correlation function at the first minimum $K_{\min}$ are listed in table 2. The general trend as the effective dimensionality is lowered is for the half-width to be reduced whilst the negative minimum increases in depth and occurs at a smaller voltage.

To study the crossovers between the limits studied above, we calculate the correlation function for arbitrary L_c by solving the diffusion equation, equation (10), in the presence of

Table 2. Parameters describing the shape of the voltage correlation function given in terms of V_c in the analytic limits. The width at half-height is V_K, the voltage at the first minimum is $V_{\min}$ and the value of the correlation function at the first minimum is $K_{\min}$.

Effective dimensionality	V_K/V_c	$V_{\min}/V_c$	$K_{\min}$
3D	0.65	3.08	−0.053
Q2D	0.53	1.73	−0.125
Q1D	0.39	1.25	−0.191
Q0D	0.38	1.00	−0.250

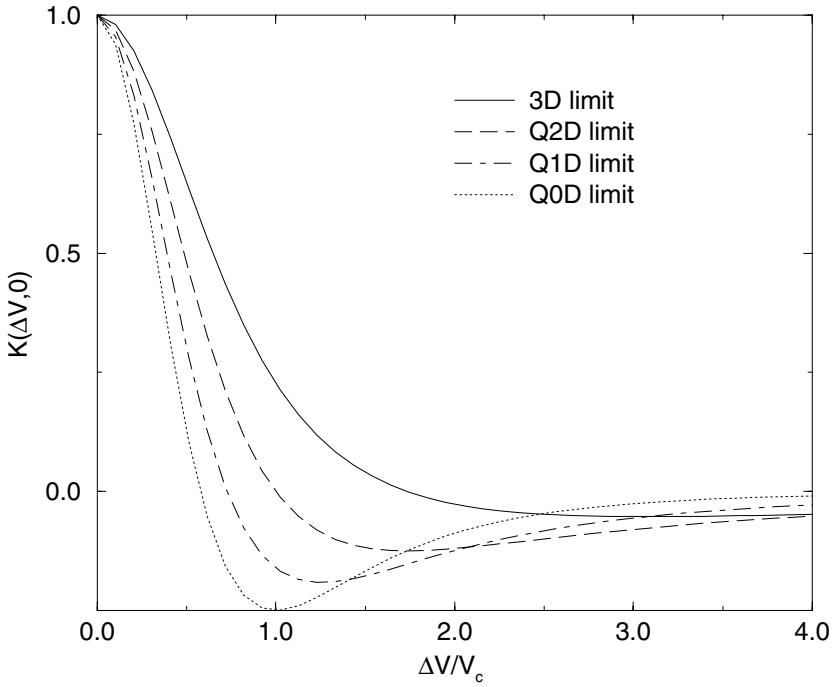

Figure 2. Analytic results for the correlation function $K(\Delta V, 0)$ as a function of $\Delta V/V_c$ in the limits of effective dimensionalities defined in table 1.

the boundary condition, equation (11). This is done by first finding the eigenvalues λ_n and normalized eigenvectors $\psi_n(\boldsymbol{r})$ of

$$\left[-\mathrm{i}\omega - D\nabla^2 + \gamma\right]\psi_n(\boldsymbol{r}) = \lambda_n\psi_n(\boldsymbol{r}) \tag{22}$$

and expressing the propagator as

$$P_\omega(\boldsymbol{r}, \boldsymbol{r}') = \sum_{n=0}^{\infty} \frac{\psi_n(\boldsymbol{r})\psi_n^*(\boldsymbol{r}')}{\lambda_n}. \tag{23}$$

In circular cylindrical coordinates the position of the resonant impurity is $\boldsymbol{r} = (\rho, \phi, z)$ with $z = 0$ as shown in figure 1. The angle ϕ is set to zero without loss of generality and we find

$$P_\omega(\boldsymbol{r}, \boldsymbol{r}) = \frac{2}{\pi R^2 L} \sum_{m,\alpha_{nm}} \frac{J_m^2(\alpha_{nm}\rho/R)}{(1 - m^2/\alpha_{nm}^2)J_m^2(\alpha_{nm})} \sum_{q_z} \frac{\cos^2(q_z z)}{(Dq_z^2 + D\alpha_{nm}^2/R^2 + \gamma - \mathrm{i}\omega)} \tag{24}$$

where $m = 0, \pm 1, \pm 2, \ldots$ and J_m is a Bessel function of the first kind of order m. For a given m, the numbers α_{nm} are solutions of the boundary condition at the cylinder surface $\rho = R$:

$$\partial_\rho J_m(\alpha_{nm}\rho/R)\big|_{\rho=R} = 0$$

which may be expressed as

$$m J_m(\alpha_{nm}) = \alpha_{nm} J_{m+1}(\alpha_{nm}).$$

We solve this boundary condition numerically in order to calculate the propagator and the correlation function for arbitrary L_c and $0 \leqslant \rho \leqslant R$.

3.1. Dimensional crossover in a thin film

First we present results for a film with $L/R = 0.3$, a geometry which is similar to that studied in the experiments of references [10, 11]. The dependence of the correlation function $K(\Delta V, 0)$ on ΔV with the spectrometer positioned at the centre of the film $\rho/R = 0$ is shown in figure 3 for representative values of L_c/R (symbols) with a comparison to the analytic limits (continuous lines). The dependence of $K(\Delta V, 0)$ on ΔV with the spectrometer positioned halfway between the centre of the film and its perimeter $\rho/R = 0.5$ is shown in figure 4. In order to quantify the change in the shape of $K(\Delta V, 0)$ as a function of L_c/R in the film, figure 5 shows the half-width V_K and the value of the correlation function at the first minimum $K_{\min}$ with numerical results for different impurity positions (symbols) compared with the analytic limits (continuous horizontal lines). The vertical lines represent the positions where we would expect a crossover between dimensionalities, namely $L_c = L$ (dashed) and $L_c = R$ (dotted).

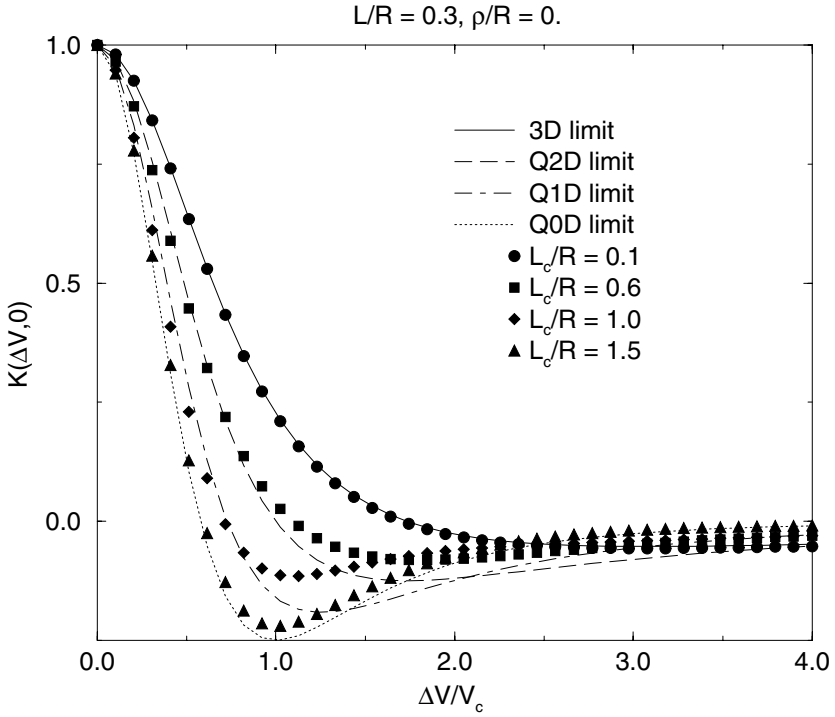

Figure 3. The theoretical form of the correlation function $K(\Delta V, 0)$ for a film with $L/R = 0.3$ as a function of $\Delta V/V_c$ with the resonant impurity on the cylinder axis $\rho/R = 0$. Continuous lines are analytic limits and symbols are numerical results for different values of L_c/R as shown in the key.

As expected, the correlation function shows 3D behaviour for $L_c \ll \{L, R\}$ and Q0D behaviour for $\{L, R\} \ll L_c$, irrespective of the impurity position. For the impurity at the centre of the film $\rho/R = 0$ (solid circles in figure 5), there is a relatively smooth change in both V_K and $K_{\min}$ as L_c increases at $L_c = L$ from their 3D values to values nearer the Q2D expectation. For $L < L_c < R$ there is a plateau in $K_{\min}$ between the 3D and Q2D values whereas V_K falls steadily towards the Q0D value and this fall is complete at $L_c = R$. The change in $K_{\min}$ to its Q0D value is much slower and is only complete at $\{L, R\} \ll L_c$. For the impurity positioned halfway between the centre of the film and its perimeter $\rho/R = 0.5$ (clear

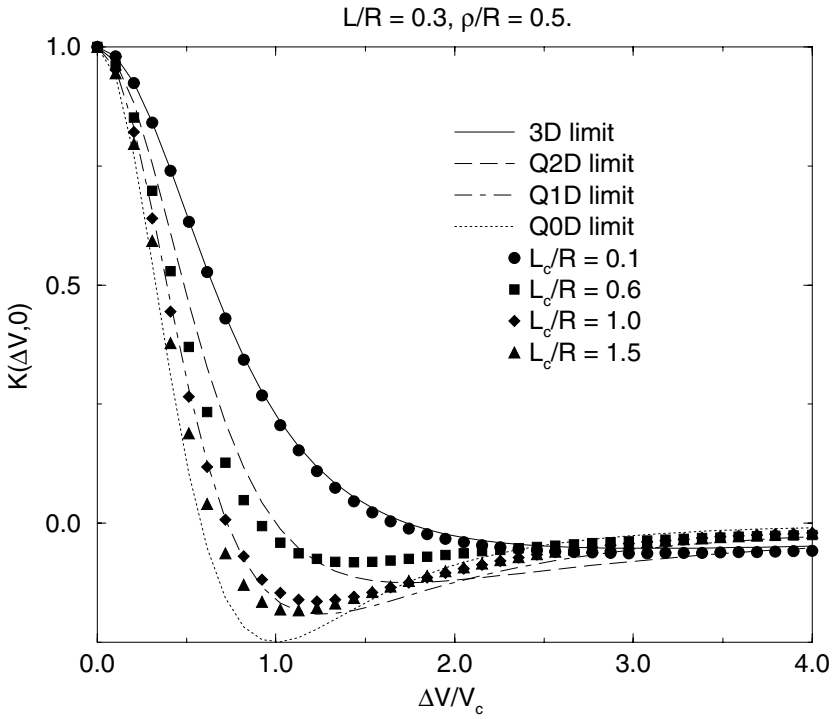

Figure 4. The theoretical form of the correlation function $K(\Delta V, 0)$ for a film with $L/R = 0.3$ as a function of $\Delta V/V_c$ with the resonant impurity off the cylinder axis $\rho/R = 0.5$. Continuous lines are analytic limits and symbols are numerical results for different values of L_c/R as shown in the key.

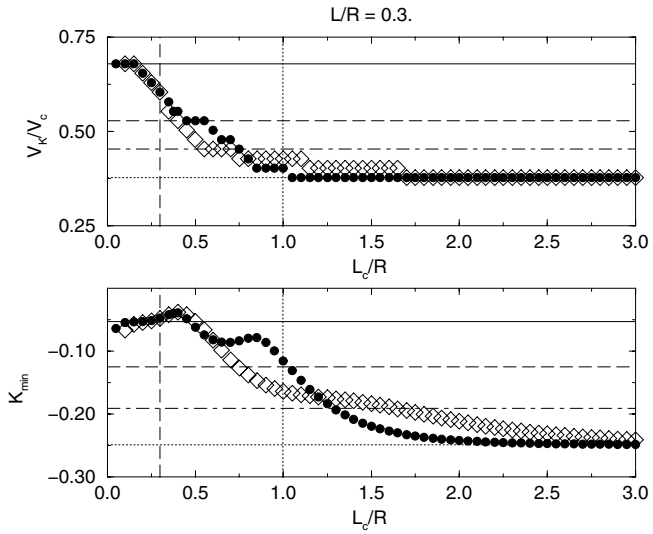

Figure 5. Numerical evaluation of the dependence on L_c of parameters describing the shape of the voltage correlation function for a film with $L/R = 0.3$. The top panel shows the width at half-height V_K and the bottom one shows the value of the correlation function at the first minimum $K_{\min}$ for $\rho/R = 0$ (solid circles) and $\rho/R = 0.5$ (clear diamonds). Horizontal continuous lines are analytic limits given in table 2: solid: 3D; dashed: Q2D; dot–dashed: Q1D; dotted: Q0D. The vertical dashed line is $L_c = L$ and the vertical dotted line is $L_c = R$.

diamonds in figure 5), there is very little difference in the shape of $K(\Delta V, 0)$ near $L_c = L$ as compared to the shape for the impurity at the centre of the film: there is no dependence on the impurity position at the crossover between 3D and Q2D because the diffusive modes in the plane of the film are not influenced by the geometry. On the other hand, there is quite a strong dependence on the impurity position at the Q2D/Q0D crossover around $L_c = R$, especially in the $K_{\min}$-values which change very slowly to their Q0D limit: in this case the diffusive modes in the plane of the film are heavily influenced by the geometry.

3.2. Dimensional crossover in a wire

Now we consider a cylindrical wire with $L/R = 3.0$. The dependence of the correlation function $K(\Delta V, 0)$ on ΔV with the spectrometer positioned on the axis of the cylinder $\rho/R = 0$ is shown in figure 6 for representative values of L_c/R (symbols) with a comparison to the analytic limits (continuous lines). The dependence of $K(\Delta V, 0)$ on ΔV with the spectrometer positioned halfway between the cylinder axis and its perimeter $\rho/R = 0.5$ is shown in figure 7. To quantify the change in the shape of $K(\Delta V, 0)$ as a function of L_c/R for the wire, figure 8 shows the half-width V_K and the value of the correlation function at the first minimum $K_{\min}$ with numerical results for different impurity positions (symbols) compared with the analytic limits (continuous horizontal lines). The vertical lines represent the positions where we would expect a crossover between dimensionality, namely $L_c = L$ (dashed) and $L_c = R$ (dotted).

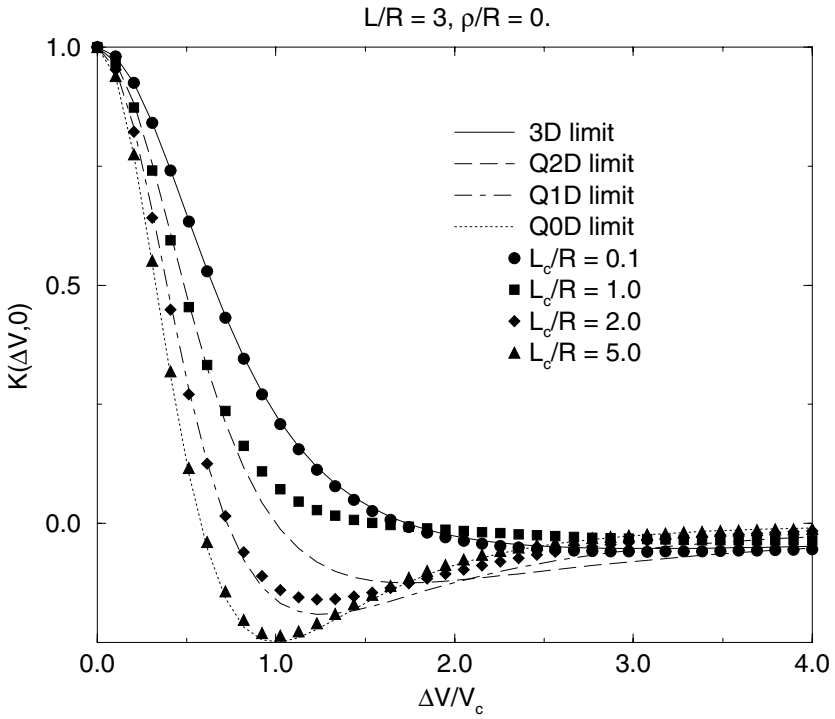

Figure 6. The theoretical form of the correlation function $K(\Delta V, 0)$ for a wire with $L/R = 3.0$ as a function of $\Delta V/V_c$ with the resonant impurity on the cylinder axis $\rho/R = 0$. Continuous lines are analytic limits and symbols are numerical results for different values of L_c/R as shown in the key.

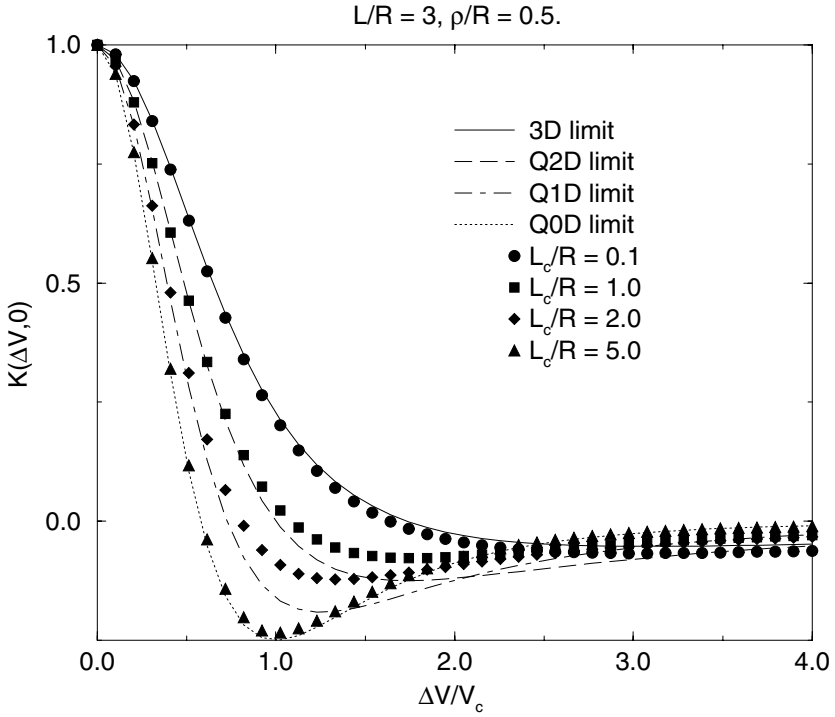

Figure 7. The theoretical form of the correlation function $K(\Delta V, 0)$ for a wire with $L/R = 3.0$ as a function of $\Delta V/V_c$ with the resonant impurity off the cylinder axis $\rho/R = 0.5$. Continuous lines are analytic limits and symbols are numerical results for different values of L_c/R as shown in the key.

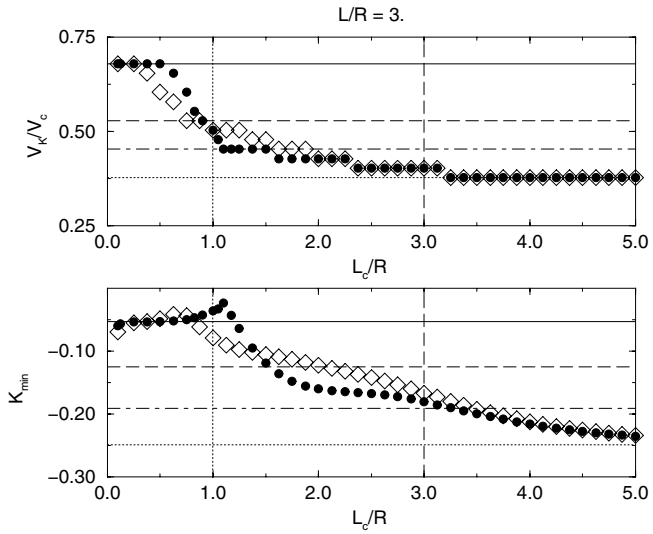

Figure 8. Numerical evaluation of the dependence on L_c of parameters describing the shape of the voltage correlation function for a wire with $L/R = 3.0$. The top panel shows the width at half-height V_K and the bottom one shows the value of the correlation function at the first minimum $K_{\min}$ for $\rho/R = 0$ (solid circles) and $\rho/R = 0.5$ (clear diamonds). Horizontal continuous lines are analytic limits given in table 2: solid: 3D; dashed: Q2D; dot–dashed: Q1D; dotted: Q0D. The vertical dashed line is $L_c = L$ and the vertical dotted line is $L_c = R$.

As for the film, the correlation function for the wire shows 3D behaviour for $L_c \ll \{L, R\}$ and Q0D behaviour for $\{L, R\} \ll L_c$, irrespective of the impurity position. For the impurity on the cylinder axis $\rho/R = 0$ (solid circles in figure 8) there is a sharp change in both V_K and $K_{\min}$ as L_c increases at $L_c = R$ from their 3D values to values nearer the Q1D expectation. For $R < L_c < L$ there seems to be a slight plateau in $K_{\min}$ just above the Q1D limit whereas V_K falls steadily towards the Q0D value and this fall is complete at $L_c = L$. The change in $K_{\min}$ to its Q0D value is much slower and is only complete at $\{L, R\} \ll L_c$. For the impurity positioned halfway between the cylinder axis and its perimeter $\rho/R = 0.5$ (clear diamonds in figure 5), the 3D/Q1D crossover is smoother than that with the impurity on the cylinder axis: as for the film, the diffusive modes perpendicular to the cylinder axis are heavily influenced by the geometry near $L_c = R$. On the other hand, there is quite weak dependence on the impurity position at the Q1D/Q0D crossover around $L_c = L$.

4. Magnetic field-dependent correlation functions

In this section we describe the calculation of the correlation function with respect to magnetic field. For convenience, a particular choice of magnetic vector potential is made for each different geometry and magnetic field orientation, preserving the zero-field boundary conditions, $\boldsymbol{n} \cdot \boldsymbol{\nabla}\psi = 0$, by choosing $\boldsymbol{A} \cdot \boldsymbol{n} = 0$ [25]. We begin by considering the field orientated parallel to the cylinder axis. In the 3D and Q2D cases, the sample is considered to be infinite in the perpendicular direction and it is convenient to adopt Cartesian coordinates and to use the Landau gauge. The vector potential may be written as $\boldsymbol{A} = \hat{\boldsymbol{j}} x\, \Delta B$ where $\hat{\boldsymbol{j}}$ is a unit vector in the y-direction, perpendicular to the axis. The zero-field boundary conditions are preserved since $\boldsymbol{A} \cdot \boldsymbol{k} = 0$ and, the sample being infinite in the y-direction, the propagator may be written as

$$P_\omega(\boldsymbol{r}, \boldsymbol{r}) = \frac{1}{L} \sum_{n=0}^{\infty} \sum_{q_z} \int_{-\infty}^{\infty} \frac{\mathrm{d}q_y}{2\pi} \frac{2\cos^2(q_z z)\varphi_n^2(x, q_y)}{(Dq_z^2 + 2D\lambda^{-2}(n + \frac{1}{2}) + \gamma - \mathrm{i}\omega)} \tag{25}$$

where $\lambda^{-2} = e\,\Delta B/c\hbar$, and $\varphi_n(x, q_y)$ are Landau wavefunctions of an electron in a magnetic field. As a result, the correlation function of differential conductances with respect to magnetic field variation directed parallel to the current $K_d^{\parallel}(0, \Delta B)$ for $d = 3, 2$ may be written as [12]

$$K_3^{\parallel}(0, \Delta B) = \sum_{n=0}^{\infty} \frac{\frac{3}{2}(X_3^{\parallel})^{-3/2}}{[n + \frac{1}{2} + 1/X_3^{\parallel}]^{5/2}} \tag{26}$$

$$K_2^{\parallel}(0, \Delta B) = \sum_{n=0}^{\infty} \frac{2(X_2^{\parallel})^{-2}}{[n + \frac{1}{2} + 1/X_2^{\parallel}]^3} = -\frac{1}{(X_2^{\parallel})^2} \psi^{(2)}\left(\frac{1}{2} + \frac{1}{X_2^{\parallel}}\right) \tag{27}$$

$$X_3^{\parallel} = X_2^{\parallel} = \frac{\Delta B}{B_{c,3\,(2)}^{\parallel}} \qquad B_{c,3\,(2)}^{\parallel} = \frac{hc}{2eL_c^2} \tag{28}$$

where $\psi^{(2)}$ is the second derivative of Euler's psi function and the factors $(X_3^{\parallel})^{-3/2}$ and $(X_2^{\parallel})^{-2}$ arise after correct normalization of the Landau wavefunctions.

As stated above, Q1D and Q0D correspond to taking into account in the diffusion propagator, equation (10), only the lowest mode, $\boldsymbol{q}_\perp = 0$, with respect to diffusion perpendicular to the cylinder axis. This corresponds to setting $\nabla_\perp = 0$. The vector potential $\boldsymbol{A}$ is treated as a perturbation [17] that is averaged with respect to the zero-mode wavefunctions for zero field:

$$\psi_0(z) = \sqrt{2/\pi L R^2}\cos(q_z z) \qquad \text{for Q1D}$$

$$\psi_0 = \sqrt{1/\pi R^2 L} \qquad \text{for Q0D}$$

which are spatially homogeneous in the perpendicular direction. To simplify, we choose $\langle \boldsymbol{A} \rangle = 0$ so that we need to calculate only

$$\langle \boldsymbol{A}^2 \rangle = \int \boldsymbol{A}^2 \psi_0^2(z)\, \mathrm{d}z\, \rho\, \mathrm{d}\rho\, \mathrm{d}\phi.$$

The diffusion equation is now expressed as

$$\left[-\mathrm{i}\omega + D\left(\frac{e}{\hbar c}\right)^2 \langle \boldsymbol{A}^2 \rangle - D\,\partial_z^2 + \gamma \right] P_\omega(\boldsymbol{r}, \boldsymbol{r}') = \delta(\boldsymbol{r} - \boldsymbol{r}'). \tag{29}$$

Providing that we also choose $\boldsymbol{A}$ without any z-dependence, we may write

$$P_\omega(\boldsymbol{r}, \boldsymbol{r}) = \frac{2}{\pi R^2 L} \sum_{q_z} \frac{\cos^2(q_z z)}{(Dq_z^2 + D(e/[\hbar c])^2 \langle \boldsymbol{A}^2 \rangle + \gamma - \mathrm{i}\omega)}$$

In order to calculate $\langle \boldsymbol{A}^2 \rangle$ we employ circular cylindrical coordinates (ρ, ϕ, z) with unit vectors $(\hat{\boldsymbol{\rho}}_0, \hat{\boldsymbol{\phi}}_0, \hat{\boldsymbol{k}})$. It is appropriate to write the vector potential in the symmetric gauge, $\boldsymbol{A} = \hat{\boldsymbol{\phi}}_0 \rho(\Delta B/2)$, because it maintains radial symmetry and obeys $\boldsymbol{A} \cdot \boldsymbol{n} \equiv \boldsymbol{A} \cdot \hat{\boldsymbol{\rho}}_0 = 0$. Thus $\langle \boldsymbol{A}^2 \rangle = \Delta B^2 R^2/8$ and we find

$$K_1^{\parallel}(0, \Delta B) = \frac{1}{[1 + (X_1^{\parallel})^2]^{5/2}} \tag{30}$$

$$K_0^{\parallel}(0, \Delta B) = \frac{1}{[1 + (X_0^{\parallel})^2]^3} \tag{31}$$

$$X_1^{\parallel} = X_0^{\parallel} = \frac{\Delta B}{B_{c,1(0)}^{\parallel}} \qquad B_{c,1(0)}^{\parallel} = \sqrt{\frac{4}{\pi}} \frac{hc}{eRL_c}. \tag{32}$$

The correlation functions in 3D and Q0D, equation (26) and equation (31) respectively, are largely insensitive to the orientation of the applied magnetic field because L_c is either smaller than all dimensions or larger than all dimensions. On the other hand, the correlation functions in Q2D and Q1D, equation (27) and equation (30) respectively, are sensitive to the orientation of the applied magnetic field because motion perpendicular to the field direction may be influenced by the boundary conditions.

For the magnetic field orientated perpendicular to the cylinder axis in Q2D and Q1D, we again treat $\boldsymbol{A}$ as a perturbation that is averaged with respect to the zero-mode wavefunctions for zero field. For Q2D we choose $\boldsymbol{A} = -\hat{\boldsymbol{j}}(z - L/2)\,\Delta B$, satisfying $\langle \boldsymbol{A} \rangle = 0$ and $\boldsymbol{A} \cdot \boldsymbol{k} = 0$, which gives $\langle \boldsymbol{A}^2 \rangle = \Delta B^2\, L^2/12$:

$$K_2^{\perp}(0, \Delta B) = \frac{1}{[1 + (X_2^{\perp})^2]^2} \tag{33}$$

$$X_2^{\perp} = \frac{\Delta B}{B_{c,2}^{\perp}} \qquad B_{c,2}^{\perp} = \sqrt{\frac{6}{\pi}} \frac{hc}{eLL_c}. \tag{34}$$

This correlation function is qualitatively different from that for a parallel magnetic field, equation (27).

For Q1D we choose $\boldsymbol{A} = \hat{\boldsymbol{k}} \rho\, \Delta B \sin\phi$ in circular cylindrical coordinates, satisfying $\langle \boldsymbol{A} \rangle = 0$ and $\boldsymbol{A} \cdot \hat{\boldsymbol{\rho}}_0 = 0$, which gives $\langle \boldsymbol{A}^2 \rangle = \Delta B^2\, R^2/4$:

$$K_1^{\perp}(0, \Delta B) = \frac{1}{[1 + (X_1^{\perp})^2]^{5/2}} \tag{35}$$

$$X_1^{\perp} = \frac{\Delta B}{B_{c,1}^{\perp}} \qquad B_{c,1}^{\perp} = \sqrt{\frac{2}{\pi}} \frac{hc}{eRL_c}. \tag{36}$$

In Q1D, the correlation functions (30) and (35) have the same form and the correlation parameters B_c for the field orientated along the wire axis and perpendicular to it may differ only by a factor of $\sqrt{2}$, $\Delta B_c^{\parallel}/\Delta B_c^{\perp} = \sqrt{2}$.

5. Summary

In this paper we presented a theoretical analysis of correlation properties of impurity-assisted tunnelling in an asymmetric double-barrier structure. The aim was to provide a means of analysing fluctuation data obtained experimentally in situations where the quasi-particle relaxation length L_c is comparable with or greater than the sample dimensions, producing an effective dimensionality less than three. We considered the change in shape of the voltage-dependent correlation function of differential conductances as L_c is varied and showed that, near a crossover between effective dimensionalities, it is influenced by the exact geometry of the sample and the position of the resonant impurity.

Acknowledgments

The authors thank R J Haug and J Könemann for discussions. This work was supported by the EPSRC and NATO CLG.

References

[1] Su B, Goldman V J and Cunningham J E 1992 *Phys. Rev.* B **46** 7644
[2] Dellow M W, Beton P H, Langerak C J G M, Foster T J, Main P C, Eaves L, Henini M, Beaumont S P and Wilkinson C D W 1992 *Phys. Rev. Lett.* **68** 1754
Geim A K, Main P C, Lascala N, Eaves L, Foster T J, Beton P H, Sakai J W, Sheard F W, Henini M, Hill G and Pate M A 1994 *Phys. Rev. Lett.* **72** 2061
McDonnell P J, Geim A K, Main P C, Foster T J, Beton P H and Eaves L 1995 *Physica* B **211** 433
[3] Tewordt M, Martín-Moreno L, Law V J, Kelly M J, Newbury R, Pepper M, Ritchie D A, Frost J E F and Jones G A C 1992 *Phys. Rev.* B **46** 3948
Tewordt M, Martín-Moreno L, Nicholls J T, Pepper M, Kelly M J, Law V J, Ritchie D A, Frost J E F and Jones G A C 1992 *Phys. Rev.* B **45** 14 407
Schmidt T, Tewordt M, Blick R H, Haug R J, Pfannkuche D, von Klitzing K, Förster A and Lüth H 1995 *Phys. Rev.* B **51** 5570
[4] Deshpande M R, Sleight J W, Reed M A, Wheeler R G and Matyi R J 1996 *Phys. Rev. Lett.* **76** 1328
Sleight J W, Hornbeck E S, Deshpande M R, Wheeler R G, Reed M A, Bowen R C, Frensley W R, Randall J N and Matyi R J 1996 *Phys. Rev.* B **53** 15 727
[5] Schmidt T, Haug R J, Fal'ko V I, von Klitzing K, Förster A and Lüth H 1996 *Europhys. Lett.* **36** 61
[6] Schmidt T, Haug R J, Fal'ko V I, von Klitzing K, Förster A and Lüth H 1997 *Phys. Rev. Lett.* **78** 1540
[7] Main P C, Thornton A S G, Hill R J A, Stoddart S T, Ihn T, Eaves L, Benedict K A and Henini M 2000 *Phys. Rev. Lett.* **84** 729
[8] Holder J P, Savchenko A K, Fal'ko V I, Joualt B, Faini G, Laruelle F and Bedel E 2000 *Phys. Rev. Lett.* **84** 1563
[9] König P, Schmidt T and Haug R J 2001 *Europhys. Lett.* **54** 495
[10] Schmidt T, König P, McCann E, Fal'ko V I and Haug R J 2001 *Phys. Rev. Lett.* **86** 276
[11] Könemann J, König P, Schmidt T, McCann E, Fal'ko V I and Haug R J 2001 *Preprint* cond-mat/0105025
[12] Fal'ko V I 1997 *Phys. Rev.* B **56** 1049
[13] Lerner I V 1988 *Phys. Lett.* A **133** 253
[14] Altshuler B L, Kravtsov V E and Lerner I V 1991 *Mesoscopic Phenomena in Solids* ed B L Altshuler *et al* (Amsterdam: North-Holland) p 449
[15] Altshuler B L and Shklovskii B I 1986 *Sov. Phys.–JETP* **64** 127
[16] Altshuler B L, Aronov A G and Spivak B Z 1981 *JETP Lett.* **33** 94
[17] Altshuler B L and Aronov A G 1981 *JETP Lett.* **33** 499
[18] Efetov K B 1983 *Adv. Phys.* **32** 53

[19] Sivan U, Milliken F P, Milkove K, Rishton S, Lee Y, Hong J M, Boegli V, Kern D and Defranza M 1994 *Europhys. Lett.* **25** 605
[20] Chaplik A and Entin M 1974 *Sov. Phys.–JETP* **40** 106
[21] Azbel M 1983 *Solid State Commun.* **45** 527
[22] Xue W and Lee P A 1988 *Phys. Rev. Lett.* **38** 3913
[23] Lerner I V and Raikh M E 1992 *Phys. Rev.* B **45** 14 036
[24] Altshuler B L, Khmelnitskii D E, Larkin A I and Lee P A 1980 *Phys. Rev.* B **22** 5142
[25] Fal'ko V I and Efetov K B 1994 *Phys. Rev.* B **50** 11 267